Inorganic Chemistry

Article

pubs.acs.org/IC

How Bonding in Manganous Phosphates Affects their Mn(II)−^{31}P Hyperfine Interactions

Sun Un* and Eduardo M. Bruch†

Department of Biochemistry, Biophysics and Structural Biology, Institute for Integrative Biology of the Cell, CEA, CNRS, Université Paris-Saclay, F-91198 Gif-sur-Yvette, France

Supporting Information

ABSTRACT: Manganous phosphates have been postulated to play an important role in cells as antioxidants. In situ Mn(II) electron−nuclear double resonance (ENDOR) spectroscopy has been used to measure their speciation in cells. The analyses of such ENDOR spectra and the quantification of cellular Mn(II) phosphates has been based on comparisons to in vitro model complexes and heuristic modeling. In order to put such analyses on a more physical and theoretical footing, the Mn(II)−^{31}P hyperfine interactions of various Mn(II) phosphate complexes have been measured by 95 GHz ENDOR spectroscopy. The dipolar components of these interactions remained relatively constant as a function of pH, esterification, and phosphate chain length, while the isotropic contributions were significantly affected. Counterintuitively, although the manganese−phosphate bonds are weakened by protonation and esterification, they lead to larger isotropic values, indicating higher unpaired-electron spin densities at the phosphorus nuclei. By comparison, extending the phosphate chain with additional phosphate groups lowers the spin density. Density functional theory calculations of model complexes quantitatively reproduced the measured hyperfine couplings and provided detailed insights into how bonding in Mn(II) phosphate complexes modulates the electron-spin polarization and consequently their isotropic hyperfine couplings. These results show that various classes of phosphates can be identified by their ENDOR spectra and provide a theoretical framework for understanding the in situ ^{31}P ENDOR spectra of cellular Mn(II) complexes.

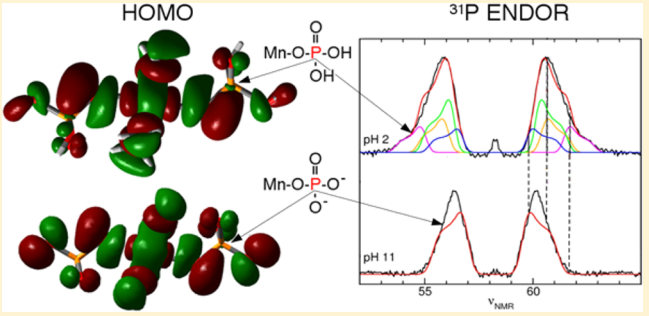

INTRODUCTION

Manganese is essential for aerobic life. It is involved in a number of important aspects of oxygen chemistry. For example, manganese superoxide dismutase (MnSOD) controls the level of superoxide, the precursor to many reactive oxygen species (ROS). In cells, manganese exists mainly in the form of Mn(II) and is found bound to a wide range of molecules from large proteins to phosphates. This latter group is diverse, ranging from simple orthophosphates (P_i) to metabolites and nucleic acids. It has been demonstrated in vitro that manganous phosphate can dismutate superoxide.[1,2] This has promoted the hypothesis that the accumulation of high levels of manganese by certain organisms, such as *Deinococcus radiodurans*, is associated with the need to control ROS.[3−5] To examine this issue, electron paramagnetic resonance (EPR) techniques have been used to measure the Mn(II) speciation in intact organisms.[6−10] Electron−nuclear double resonance (ENDOR) spectroscopy has shown that phosphates are one of the major ligands. The ^{31}P ENDOR spectra of Mn(II) centers in organisms exhibit partially resolved complex shapes.[6−8,10] Comparison to model complexes indicated that the line shape was consistent with Mn(II) bound to the phosphate groups of nucleic acids, fructose-1,6-bisphosphate, and inorganic phosphates.[7,10] Measurements on *Arabidopsis* seeds indicated that the ^{31}P ENDOR spectra of Mn(II) phosphates were sensitive to the variation in pH among different organelles.[10]

This model-driven empirical approach has more than adequately explained the ^{31}P ENDOR spectra of cells. It has suggested that there is a close relationship between the structure of the phosphate ligand and the hyperfine interaction (A^{31}_{P}) between the $S = {}^5/_2$ Mn(II) electronic spin and the spin-$^1/_2$ ^{31}P nucleus. ^{31}P ENDOR spectra have been obtained for a diverse number of Mn(II) centers and are well-understood.[11−15] They are characterized by a simple doublet (see Figure 1) that arises from the Mn(II)−^{31}P hyperfine interaction. The splitting ranges from 4 MHz for simple phosphates to more than 9 MHz for Mn(II) bound to nucleic acids (e.g., see refs 16 and 15). A^{31}_{P} is the sum of its isotropic ($A^{31}_{P,iso}$) and anisotropic ($T^{31}_{P,nn}$, $n = x, y, z$) components. The isotropic hyperfine interaction arises from polarization effects that result in a net electron spin density at the nucleus and thus depends on factors affecting the bonding between the ligand and Mn(II), though not necessarily in a straightforward manner. $T^{31}_{P,nn}$ largely arises from the magnetic dipole−dipole

Received: August 14, 2015
Published: October 21, 2015

DOI: 10.1021/acs.inorgchem.5b01864
Inorg. Chem. 2015, 54, 10422−10428

coupling between the manganese electron spin and the ^{31}P nuclear spin, which depends on the interspin distance r (as r^{-3}) and orientation. Most of the differences in the ^{31}P ENDOR spectra of phosphates arise from the isotropic component. ^{31}P orthophosphate nuclei have $A^{31}_{P,iso}$ values of about 5 MHz at a distance of 3.3 Å from the Mn(II) center. An interesting point of comparison is the water-ligand protons, which have $A^{1}_{H,iso}$ values of less than 1 MHz[17,18] at a shorter distance of 2.7 Å. By contrast, the dipolar coupling constants are nearly the same once the distance and differences in the nuclear magnetic moments are taken into consideration. In both cases, an intervening oxygen atom mediates the polarization of the spin density. These observations suggest that Mn(II)−O−P bonding promotes spin polarization at the phosphorus atom.

What has been lacking is a more quantitative understanding of the manganese−phosphate hyperfine interaction that would help relate these observations to the structure and bonding of the manganese phosphate complexes. Such knowledge would not only help define the limits of using model data but also potentially provide detailed information, beyond simple speciation, about the physical and chemical states of the various cellular Mn(II) phosphates. To accomplish this, we have carried out ^{31}P ENDOR measurements on a series of simple phosphates and compared their experimentally determined ^{31}P hyperfine couplings with those obtained from density functional theory (DFT) calculations. A similar approach has been used previously to study the manganese−phosphate interactions in aluminophosphate zeotypes.[11] As will be described, for the simpler phosphates that we have examined, the agreement between measurements and DFT calculations was nearly quantitative. This has allowed us to determine how factors such as protonation, ionic interactions, and esterification affect the Mn(II)−^{31}P hyperfine interactions and manganese−phosphate bonding and to understand how spin polarization is mediated. Using this information, we have been able to better define the extent to which ^{31}P ENDOR spectroscopy can be exploited to examine Mn(II) phosphate speciation in cells.

EXPERIMENTAL SECTION

Model Complexes. In the following, all of the solutions contained Mn(II) from $Mn(ClO_4)_2{\cdot}6H_2O$ (Sigma-Aldrich) and were pH-adjusted using HCl and KOH. For orthophosphate measurements, solutions contained 50 μM Mn(II): for pH 11, Mn(II) was mixed with 100 mM KP_i and 100 mM CAPS/KOH immediately prior to freezing in order to prevent oxidation; for pH 7, 50 mM KP_i in 200 mM HEPES/KOH was used; for pH 2, concentrated phosphoric acid (85%) diluted to approximately 500 mM was employed. The ^{31}P ENDOR spectra showed that each of the complexes had two or three phosphate groups per Mn(II). The 1:1 Mn(II) adenosine phosphates were obtained by mixing 100 μM Mn(II) with 100 mM adenosine monophosphate (AMP), 100 μM adenosine diphosphate (ADP), and 100 μM adenosine triphosphate (ATP) in 100 mM HEPES (pH 7). The 1:2 Mn(II) dimethylphosphophosphate (DMP) complexes were obtained by adding 50−100 μM Mn(II) to a 100 mM aqueous solution of DMP adjusted to pH 8−7. In all cases, the 285 GHz EPR spectra indicated the presence of a single dominant complex. The water and phosphate ligand stoichiometries were determined using a modified version of the method of Potapov and Goldfarb.[7,19]

EPR Spectroscopy. The 95 GHz electron−electron double resonance (ELDOR)-NMR and ENDOR spectra were obtained at 6 K using a Bruker Elexsys II 680 EPR spectrometer equipped with a Bruker "Power Upgrade 2", a 500 W Amplifier Research radio-frequency amplifier, and an Oxford Instruments CF935 flow cryostat. Davies ENDOR[20] measurements were composed of a 200 ns microwave π pulse followed by a 20 μs radiofrequency pulse, and the signal was detected using two-pulse $^{\pi}/_{2}-\tau-\pi$ spin−echo detection (where $^{\pi}/_{2}$ = 10 ns, π = 20 ns, and τ = 400 ns). The ^{31}P Davies ENDOR spectra were symmetrized about the ^{31}P NMR frequency of about 58.2 MHz. A typical example of unsymmetrized raw data is shown in Figure S1 in the Supporting Information. The slight asymmetries in the doublet spectra tended to be frequency-dependent, suggesting that they were mostly an instrument artifact. The symmetrized spectra were simulated using locally written programs that took into account a well-known "blind spot" toward the center of the spectrum.[21] The ELDOR-NMR[22] spectrum was obtained using the same sequence and microwave powers as in our previous measurements:[17] a 60 μs pump pulse followed by $^{\pi}/_{2}-\tau-\pi$ spin−echo detection (where $^{\pi}/_{2}$ = 300 ns, π = 600 ns, and τ = 1200 ns) . Simulations of the Davies ^{31}P ENDOR spectra were obtained using locally written programs that took into account the length of the microwave preparation pulse and the associated blind spot.[21]

DFT Calculations. DFT calculations were carried out using Gaussian 09 (revision B.01)[23] and ORCA.[24] The former was used to optimize geometries using the B3LYP hybrid density functional[25−28] and the 6-31+G(d,p) basis set[29−32] with default options. The latter was used to obtain the hyperfine coupling values using the PBE0 functional[33] and the 6-31+G(d,p) basis set[29−32] with the tightSCF and Grid5 options. All of the calculations included water solvation. For Gaussian 09 calculations, the default polarizable continuum model using the integral equation formalism was used,[34] and for Orca calculations, the COSMO model was employed.[35] Normal mode analysis showed that all of the geometries were stationary points. Molecular orbitals were drawn using the program MOLDEN.[36]

RESULTS AND DISCUSSION

Figure 1 shows frozen-solution ^{31}P Davies ENDOR spectra of Mn(II) orthophosphate ($[Mn(H_xPO_4)_2(H_2O)_4]^{+2x-4}$) obtained as a function of pH. The actual ligand stoichiometries were determined from the amplitudes of the ^{31}P and ^{1}H ENDOR spectra: two or three phosphates with corresponding four or three waters. The detected centers were more complex and extended than their nominal formulas, involving inter-

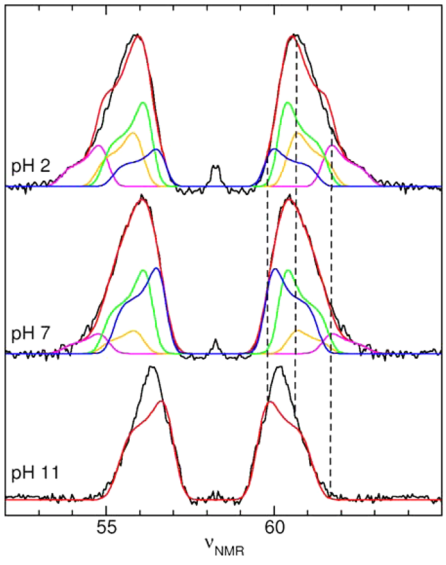

Figure 1. pH dependence of the 6 K Davies ^{31}P ENDOR spectra of Mn(II) in orthophosphate solutions (black) and simulations based on DFT hyperfine couplings (red). For the pH 2 and 7 simulations, the blue, green, orange, and magenta traces correspond to the four components listed in Table 1.

DOI: 10.1021/acs.inorgchem.5b01864
Inorg. Chem. 2015, 54, 10422−10428

actions with other ions. The Mn(II) ELDOR-NMR[22] spectra had various resonances arising from K^+, Na^+, and Cl^- (Figure 2) depending on their concentrations. This is similar to what

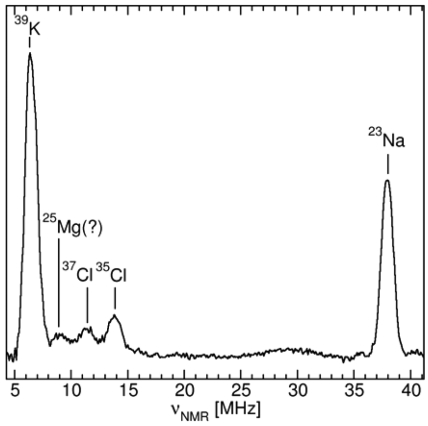

Figure 2. 6 K Mn(II) ELDOR-NMR spectrum of 100 μM Mn(II) in 150 mM phosphate solution (pH 7.2) containing 200 mM K^+, Na^+, and Cl^-. The calculated NMR frequencies of the relevant isotopes are shown.

has been observed for Mn(II) carbonate complexes, where nearby Na^+ was detected by ENDOR.[37] The K^+ and Na^+ resonances were detected only when a phosphate ligand was present, suggesting that they were ionically interacting with the negatively charged ligand. A small resonance corresponding to the NMR resonance frequency of ^{25}Mg was also detected, possibly arising from small amounts of contaminating ions or due to a detection artifact arising from the intense ^{39}K signal, similar to the even smaller resonances that flank the ^{23}Na signal. Since directly bonded Cl^- ions have broader Mn(II) ELDOR-NMR resonances,[17] the $^{35/37}$Cl resonances apparently arose from secondary sphere interactions.

As can be seen from Figure 1, the ^{31}P ENDOR spectra exhibited a strong dependence on pH. At pH 11, the resonances were the narrowest, and the apparent A_{iso} was about 3.8 MHz. Each of the doublets had a full width at half-height of about 2.7 MHz, corresponding to a dipolar coupling of about 0.9 MHz. As the pH was lowered, the doublet spacing increased, as did the width of the resonances. The pH 2 spectrum had a minor component with an apparent splitting of about 8 MHz, compared with the splitting of 4.8 MHz for the major component. Ideally, the protonation state of the phosphate groups could have been assessed using the ^{1}H ENDOR spectra of the complexes. The spectra did change as a function of pH. However, distinguishing protonation from other changes to the ligand sphere was difficult since it was also evident that the hyperfine couplings of water ligand protons themselves were also affected, as were those of second-sphere "matrix" protons.

It was reasoned that if the trend of increasing A_{iso} with decreasing pH were due to the charge of the phosphate ligand, then esterification of the phosphates should lead to similar results. As shown in Figure 3, the spectra of adenosine monophosphate (AMP) and dimethylphosphate (DMP) were consistent with this hypothesis. Both had apparent A_{iso} values that were larger than that of the P_i complex at neutral pH. The DMP complex had a minimum A_{iso} of 6 MHz. Its ENDOR resonances were broad, suggesting multiple components, some having large A_{iso} values. The inverse relationship between A_{iso}

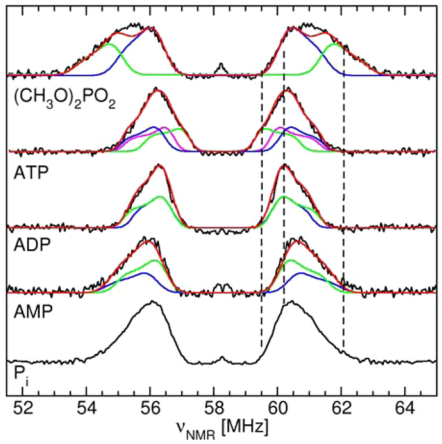

Figure 3. 6 K Davies ^{31}P ENDOR spectra of Mn(II) complexes of P_i, AMP, ADP, and ATP at pH 7.0 and of dimethylphosphate at pH 8.5. The red traces are the sums of the fitted component spectra shown in blue and green and also magenta for the ATP complex. See the text for details.

and the charge of the phosphate ligand was counterintuitive since the reduction of the phosphate charge would presumably have weakened the bonding interaction between the phosphate and the Mn(II), leading to longer bond distances and a reduction in Mn(II) spin density at the phosphorus nuclei. It was also not apparent why extending the phosphate chain, as in the case of ADP and ATP, caused the opposite trend. Nonetheless, it was this trend that made P_i, ADP, ATP, and polyphosphate complexes in organisms difficult to distinguish on the basis of their ^{31}P ENDOR spectra.[6,7,10]

To understand these effects more quantitatively, DFT calculations were carried out to determine the relationship among the ligand structure, charge, and $A^{31}_{P,iso}$. For the most part, the $A^{31}_{P,iso}$ values were a local property, but the presence of other ligands did exert a modest effect. For example, the difference in the A^{31}_{P} tensors of $[Mn(H_2PO_4)(H_2O)_5]$ and $[Mn(H_2PO_4)_2(H_2O)_4]$ was about 0.3 MHz in their $A^{31}_{P,iso}$ values. Similar size effects were also associated with additional ionic interactions between monocations and the phosphate groups. In other calculations that were carried out, the A^{31}_{P} values were even less affected by the presence of other types of ligands (e.g., nucleobases). The calculated hyperfine tensors accounted for nearly all of the features of the measured spectra (Table 1).

The DFT hyperfine values were directly used to simulate the experimental spectra (Figure 1). The amplitudes of the components were scale to obtain the best visual fit. For the cases that significantly deviated from the observed spectra, the DFT derived isotropic values were adjusted, followed by, if necessary, changes to the individual dipolar elements. Only small changes to the DFT values were required to achieve agreement with the experimental results. In the case of the pH 11 spectrum, the DFT and simulation values were very close, the main difference being 0.5 MHz in the A_{yy} value. The overall line shapes were different, probably as a result of a distribution of structures trapped in the frozen solution. At pH 7 and 2, the extent and line shape could be simulated by using values for the HPO_4^{2-}, $H_2PO_4^-$, and H_3PO_4 ligands obtained from averages of the DFT hyperfine couplings for the $[Mn(HPO_4)(PO_4)(H_2O)_4]^{3-}$, $[Mn(H_3PO_4)(H_2PO_4)(H_2O)_4]^+$, and $[Mn(H_3PO_4)_2(H_2O)_4]^{2+}$ model structures. Two different optimized

DOI: 10.1021/acs.inorgchem.5b01864
Inorg. Chem. 2015, 54, 10422−10428

Table 1. Measured and PBE0/6-31+G(d,p)-Calculated $A^{31}_{P,iso}$ and (in Parentheses) $T^{31}_{P,nn}$ Values (Details of the Structures are Listed in the Supporting Information)

model molecule	A^{31}_P [MHz] DFT[a]	A^{31}_P [MHz] simulation[b]	measured complex
$[Mn(H_2PO_4)(H_2O)_5]^+$	5.1 (−1.2, −0.6, 1.8)		
$[Mn(NaPO_4)_2(H_2O)_4]^{2-}$	4.1 (−1.2, −0.8, 1.9)		
$[Mn(PO_4)_2(H_2O)_4]^{4-}$	3.9 (−1.2, −0.8, 1.9)[c]	3.7 (−1.0, −1.0, 2.1)	$[Mn(H_xPO_4)_2(H_2O)_4]^{+2x-4}$ at pH 11
$[Mn(HPO_4)(PO_4)(H_2O)_4]^{3-}$	4.1 (−1.1, −0.8, 2.0) 4.8 (−1.1, −0.8, 1.8)	4.1 (−1.1, −0.8, 2.0) 4.9 (−1.1, −0.8, 1.8)	$[Mn(H_xPO_4)_2(H_2O)_4]^{+2x-4}$ at pH 7
$[Mn(HPO_4)_2(H_2O)_4]^{2-}$	5.0 (−1.1, −0.8, 1.8)[c]	5.4 (−1.2, −0.6, 1.7) 7.5 (−1.1, 0.7, 1.7)[d]	
$[Mn(H_2PO_4)_2(H_2O)_4]$	5.4 (−1.2, −0.6, 1.7)		
$[Mn(H_3PO_4)(H_2PO_4)(H_2O)_4]^+$	5.4 (−1.2, −0.6, 1.8) 7.0 (−1.1, −0.5, 1.6)[d]	4.1 (−1.1, −0.8, 2.0) 4.9 (−1.1, −0.8, 1.8)	$[Mn(H_xPO_4)_2(H_2O)_4]^{+2x-4}$ at pH 2
$[Mn(H_3PO_4)_2(H_2O)_4]^{2+}$ each phosphate donates a hydrogen bond to a water ligand	7.5 (−1.2, −0.6, 1.8)[d] 7.8 (−1.2, −0.6, 1.8)[d]	5.4 (−1.2, −0.6, 1.7) 7.5 (−1.1, −0.7,1.7)[d]	
$[Mn(H_3PO_4)_2(H_2O)_4]^{2+}$ each phosphate accepts a hydrogen bond from a water ligand	8.8 (−1.2, −0.6, 1.8) 9.2 (−1.2, −0.6, 1.8)		
$[Mn(CH_3OPO_3)(H_2O)_5]$ two water ligands donate a hydrogen bond to two P−O	4.8 (−1.3, −0.6, 2.0)	1:1 combination of DFT values	1:1 Mn(II):AMP complex at pH 7
$[Mn(CH_3OPO_3)(H_2O)_5]$ one water ligand donates a hydrogen bond to P−OCH_3 and another to P−O	5.4 (−1.2, −0.8, 2.0)		
$[Mn((CH_3O)_2PO_2)_2(H_2O)_4]$ both configuration 1	5.0 (−1.2, −0.6, 1.8)[c]	4.8 (−1.2, −0.6, 1.8) 7.4 (−1.1, −0.6,1.8)	1:2 Mn(II):DMP complex at pH 8
$[Mn((CH_3O)_2PO_2)_2(H_2O)_4]$ one configuration 1 and one configuration 2	5.3 (−1.2, −0.6, 1.8) 6.3 (−1.1, −0.7, 1.9)		
$[Mn((CH_3O)_2PO_2)_2(H_2O)_4]$ both configuration 2	6.3 (−1.1, −0.7, 1.8)[c]		
$[Mn((CH_3O)_2PO_2K)_2(H_2O)_4]^{2+}$ both configuration 2	6.6 (−1.1, −0.7, 1.8)[c]		
$[Mn(methyldiphosphate)(H_2O)_4]^-$	4.0 (α) (−1.1, −0.6, 1.8) 4.1 (β) (−1.2, −0.8, 2.0)	4.1[e] (−1.2, −0.3, 1.5) 4.3[e] (−1.4, −0.5, 1.9)	1:1 Mn(II):ADP complex at pH 7
$[Mn(methyltriphosphate)(H_2O)_4]^{2-}$ bidentate	4.2 (β) (−1.1, −0.6, 1.8) 4.0 (γ) (−1.2, −0.8, 2.0)	4.3[e] (−1.3, −0.7, 2.1) 3.7[e] (−1.5, −0.6, 2.2)	1:1 Mn(II):ATP complex at pH 7
$[Mn(methyltriphosphate)(H_2O)_3]^{2-}$ tridentate	4.1 (α) (−1.2, −0.7, 1.9) 3.1 (β) (−1.2, −0.6, 1.8) 4.4 (γ) (−1.3, −0.4, 1.7)	4.2[e] (−1.2,-0.7, 1.9) 3.1[e] (−1.2, −0.6, 1.8) 4.7[e] (−1.3, −0.4, 1.7)	1:1 Mn(II):ATP complex at pH 7

[a]All of the calculations were carried out on molecules embedded in water. [b]The corresponding simulations are shown in Figures 1 and 3. [c]Average of the two sets of DFT values for the two ligands. [d]Values used in the solution are the averages of three sets of DFT values for the H_3PO_4 ligand. [e]The components were fitted with equal weights.

DOI: 10.1021/acs.inorgchem.5b01864
Inorg. Chem. 2015, 54, 10422−10428

geometries were found for $[Mn(H_3PO_4)_2(H_2O)_4]^{2+}$, corresponding to two different internal hydrogen-bonding geometries: in one, each phosphate acts as a donor to a water ligand, and in the other (the reverse case), they act as acceptors. The A_{iso} values of the latter were 8.8 and 9.2 MHz, but there was no evidence of such large components in the pH 2 phosphate spectra. Hence, none were included in the simulations. The changes in going from pH 7 to 2 followed the expected changes in the relative concentrations of HPO_4^{2-}, $H_2PO_4^-$, and H_3PO_4 molecules in solution. Of course, there was no way to determine whether the fits shown in Figure 1 were unique. Because of the lack of spectral resolution, it was likely that the measured spectra could have been fitted using other hyperfine tensors and different contributions; however, the fact that the DFT-calculated tensors could account for the pH dependence in such a straightforward manner was a strong indication that the theoretical hyperfine tensors were of quantitatively predictive value.

This was supported by the equally good agreement obtained for the Mn(II) complexes of AMP, ADP, and ATP. The AMP spectra could be directly simulated using the DFT-derived hyperfine values for the two different configurations of hydrogen bonding between the water and AMP ligands (see below). The theoretical values for the ADP and ATP complexes were within 0.3 MHz of the fits shown in Figure 2 (also see Table 1). The DFT values from the tridentate model of ATP were significantly different from those of the bidentate model and closer to measured values. In particular, the A_{iso} value of 3.1 MHz for the β-phosphate group was required in order to fit the inside edges of the ENDOR spectra. In a previous study,[19] it was concluded that only a single axial component with A_{iso} = 4.5 MHz and $T^{31}_{P,\perp}$ = 0.8 ± 0.1 MHz ($T^{31}_{P,xx} = T^{31}_{P,yy}$) was required to simulate the ADP spectrum. However, these previous simulations did not fully account for the outer edges of the measured spectrum. The DFT calculations did show that the two ^{31}P hyperfine couplings are likely to be only slightly different, but they also showed that, as with all of the phosphates listed in Table 1, the dipolar components were far from axial. For a typical Mn(II) phosphate Mn−P distance of 3.2 Å, the dipolar coupling tensor based on the point-dipole approximation is $\mathbf{T}^{31}_P$ = (−0.9, −0.9, 1.8) MHz, close to the values shown in Table 1. However, this approximation neglects the appreciable shape and size of the Mn(II) d orbitals (see below), which the DFT calculations do not ignore and which account for anisotropic dipolar coupling. The same previous study also found that the ^{31}P ENDOR spectrum ATPγS could be simulated using a hyperfine tensor with A_{iso} = 4.5 MHz and $\mathbf{T}^{31}_P$ = (−1,7, −0.2, 1.9) MHz, but because of the large anisotropy they rejected this possibility in favor of two axial tensors (A_{iso} = 4.9 MHz, $T_\perp$= 0.7 MHz and A_{iso} = 3.5 MHz, $T_\perp$= 0.7 MHz). However, they poorly accounted for the inner edges of the measured spectra. By contrast, inclusion of three different anisotropic hyperfine tensors very similar to the DFT values yielded a good fit of the measured spectrum.

The largest discrepancies between our simulations and the calculations were for the [Mn(II) $(DMP)_2(H_2O)_4$] complex. As shown in Figure 4, a DMP can ligate Mn(II) in two different orientations distinguished by how adjacent water ligands donate hydrogen bonds. The hyperfine tensor of the DMP ligand with both esters accepting hydrogen bonds (configuration 2) had an A_{iso} value that was 1.4 MHz larger than that of the ligand with only one hydrogen-bonded ester oxygen (configuration 1). In addition to the one shown, we considered

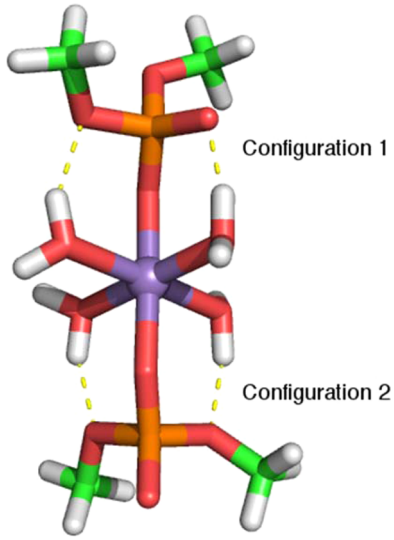

Figure 4. Two configurations of the dimethylphosphate ligands bound to Mn(II).

two other structures: in one, both DMP ligands were in configuration 2, and in the other both were in configuration 1. Thermochemical calculations showed that the three structures were within 1 kcal/mol of each other, with the one having both DMP ligands in configuration 2 being the most stable. The measured [Mn(II)$(DMP)_2(H_2O)_4$] spectrum was consistent with both configurations being present. The $A^{31}_{P,iso}$ value for the configuration-2 component (green trace in Figure 3) was 1 MHz greater than the DFT value, while that of the configuration-1 component was 0.5 MHz smaller than its corresponding calculated value. The addition of two potassium ions to the model improved the agreement with the larger tensor by 0.2 MHz. In general, the effect of ionic interactions on the hyperfine interaction appeared to be significantly smaller than that of protonation.

It was evident from the experimental data and DFT calculations that although the $T^{31}_{P,nn}$ components remained essentially constant indicating that the distances and the orientations of the ^{31}P nuclei with respect to the Mn(II) centers were unaffected, reducing the charge of a phosphate ligands did lead to higher $A^{31}_{P,iso}$ value. That is, as discussed above, spin polarization at the ^{31}P nucleus increases as the manganese−phosphate bond weakens. Consistent with this, the Mn−O(P) bond in the optimized geometries lengthened while the P−O(Mn) bond shortened linearly with increasing protonation (Figure 5). The changes in the highest-occupied molecular orbital (HOMO) illustrated what occurred at the level of the orbitals. In the absence of protonation, the HOMO was characterized by σ antibonding involving the Mn d_{z^2} orbital and p_z orbitals of all four oxygens with little involvement from the phosphorus atom (Figure 6). When the oxygens became protonated, they ceased to contribute a p_z orbital to the HOMO, which became more P−O−Mn-centered with increased participation from the phosphorus orbitals, notably its 3s orbital. It is this latter contribution that caused the increase in $A^{31}_{P,iso}$, while the counterbalancing changes in the Mn−O(P) and (Mn)O−P bond lengths left the Mn−P distance and consequently the dipolar component of the ^{31}P hyperfine interaction relatively unchanged (Figure 5). By comparison, the orbitals of water protons did not participate in five half-occupied molecular orbitals. Like the phosphate

DOI: 10.1021/acs.inorgchem.5b01864
Inorg. Chem. 2015, 54, 10422−10428

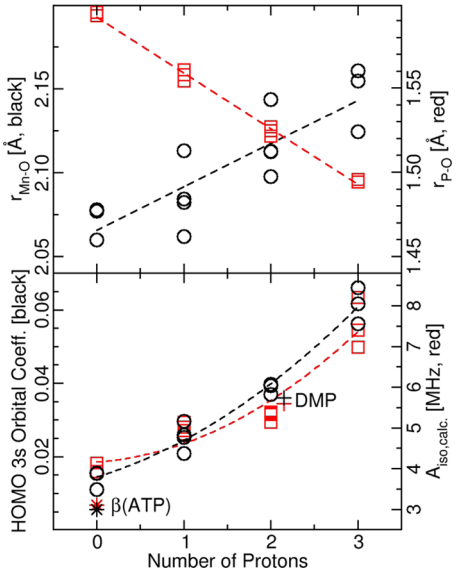

Figure 5. Effect of phosphate protonation on the structure and electronic properties of Mn(II) complexes as determined from the DFT calculations (Table 1). Regression fits of the data (dashed lines) show their trends but otherwise have no physical significance. The values for the unprotonated β-phosphate group of ATP (asterisks) and DMP (plus signs) have been added for comparison.

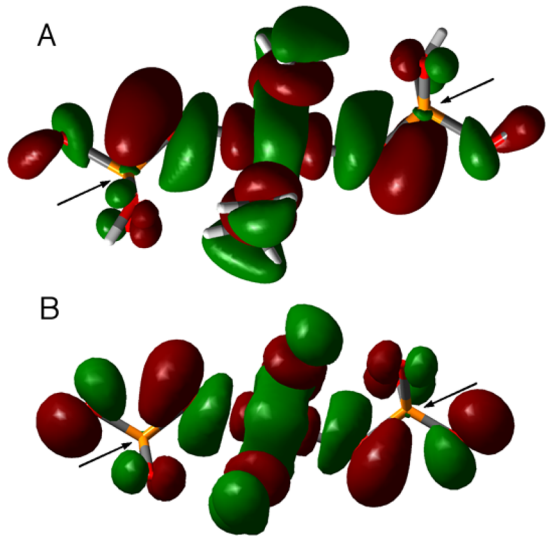

Figure 6. HOMOs of (A) $Mn(H_2PO_4)_2(H_2O)_4]$ and (B) $Mn(PO_4)_2(H_2O)_4]^{2-}$. The arrows indicate the phosphorus atoms and the s-orbital contributions. The surface cutoffs were 0.0150 e^-/au^3.

oxygens, the water oxygen p orbitals of the HOMO were involved in σ antibonding with the Mn d_{z^2} orbital, with the water proton nearly in the nodal plane of the oxygen p orbitals. This explained why the phosphorus and proton nuclei, although having similar anisotropic hyperfine components and similar distances from the metal center, had different isotropic couplings.

Esterification, in much the same way as protonation, reduced the contribution of the ester oxygen p_z orbital to the HOMO while increasing the σ-bonding character. This can be seen in Figure 5. The 3s orbital contribution for the DMP complex (black + symbol in Figure 5) is very close to that for the doubly protonated orthophosphate. By comparison, extending the phosphate chain (e.g., to diphosphate and triphosphate) had the opposite effect, increasing the bonding network through the oxygen p_z orbitals and decreasing the 3s orbital contributions of the phosphorus atom. This is evident in the case of the ATP β-phosphate group, modeled as methyltriphosphate in the DFT calculations. Its 3s orbital contribution and $A^{31}_{P,iso}$ value (the black and red asterisks, respectively, in Figure 5) were less than those of the completely deprotonated orthophosphate ligand. Extending the phosphate chain had a smaller effect than protonation/esterification, which explained why the ^{31}P ENDOR spectra of polyphosphates more closely resembled those of orthophosphates.

CONCLUSIONS

These insights into the nature of the ^{31}P hyperfine interactions have consequences for understanding the speciation of manganous phosphate complexes and their biochemical roles. They provide a theoretical basis for analyzing the speciation of Mn(II) phosphates. Previous results and those presented here show that although it is unlikely that individual Mn(II) phosphate species in organisms can be discriminated by ENDOR spectroscopy, speciation of the Mn(II) phosphates on the basis of their degree of esterification can be achieved readily by analyzing the line shapes of the ^{31}P ENDOR resonances. This of course critically depends on the quality and resolution of the data. The Mn(II) ^{31}P ENDOR spectra for all of the organisms that have been measured to date have had very similar line shapes. This shape is indicative of diverse speciation involving metabolites and nucleic acids.[6−8,10] Heuristic models[6,8] that largely ignore this information will at the very least be less informative. The nearly quantitative agreement between the DFT calculations and experimentally measured ^{31}P hyperfine couplings provides a strong theoretical justification for analyzing the line shapes of the ^{31}P ENDOR spectra of organisms in terms of three contributions: (1) ortho-, di-, tri-, and polyphosphates together as a single group; (2) sugar phosphates (monoesters); and (3) nucleic acids (diester). Such an approach is strengthened by imposing constraints arising from known concentrations of the various phosphates, as is the case for fructose-1,6-biphosphate in bacteria and yeast and phytate in seeds. As has been demonstrated previously[10] and here, the pH dependence of the ^{31}P hyperfine interaction is significant and cannot be ignored, especially in complex organisms such as yeast and seeds, in which different organelles have different pHs. On the other hand, in a manner similar to ^{31}P chemical shifts, it should be possible to use the A^{31}_{P} value of manganous phosphates as a sensor of changes in cellular pH.[38] Such an application would make Mn(II) ^{31}P ENDOR spectroscopy a useful tool for studying cellular physiology.

ASSOCIATED CONTENT

Supporting Information

The Supporting Information is available free of charge on the ACS Publications website at DOI: 10.1021/acs.inorgchem.5b01864.

An example of a raw 6 K Davies ^{31}P ENDOR spectrum of Mn(II) in orthophosphate solution and the atomic coordinates of the optimized geometries of the complexes in Table 1 (PDF)

AUTHOR INFORMATION

Corresponding Author

*E-mail: sun.un@cea.fr.

DOI: 10.1021/acs.inorgchem.5b01864
Inorg. Chem. 2015, 54, 10422−10428

Present Address

†E.M.B.: Institut Pasteur, Unité de Microbiologie Structurale and CNRS UMR 3528, Paris 75724, France.

Notes

The authors declare no competing financial interest.

■ ACKNOWLEDGMENTS

This work was partially financed by the ANR (Contracts 2011 BSV5-013-01 and 2011 BSV6-004-01), the French Infrastructure for Integrated Structural Biology (FRISBI, ANR-10-INSB-05-01), and the CNRS "Interface PCB" Program. The spectrometer was funded by the Région Ile-de-France "Sesame" Program, the CEA, and CNRS. We thank Leandro Tabares and F. Leach for their input.

■ REFERENCES

(1) Barnese, K.; Gralla, E. B.; Cabelli, D. E.; Valentine, J. S. *J. Am. Chem. Soc.* **2008**, *130*, 4604−4606.
(2) Barnese, K.; Gralla, E. B.; Valentine, J. S.; Cabelli, D. E. *Proc. Natl. Acad. Sci. U. S. A.* **2012**, *109*, 6892−6897.
(3) Daly, M. J.; Gaidamakova, E. K.; Matrosova, V. Y.; Vasilenko, A.; Zhai, M.; Venkateswaran, A.; Hess, M.; Omelchenko, M. V.; Kostandarithes, H. M.; Makarova, K. S.; Wackett, L. P.; Fredrickson, J. K.; Ghosal, D. *Science* **2004**, *306*, 1025−1028.
(4) Tseng, H.-J.; Srikhanta, Y.; McEwan, A. G.; Jennings, M. P. *Mol. Microbiol.* **2001**, *40*, 1175−1186.
(5) Archibald, F. S.; Fridovich, I. *J. Bacteriol.* **1981**, *145*, 442−451.
(6) McNaughton, R. L.; Reddi, A. R.; Clement, M. H. S.; Sharma, A.; Barnese, K.; Rosenfeld, L.; Gralla, E. B.; Valentine, J. S.; Culotta, V. C.; Hoffman, B. M. *Proc. Natl. Acad. Sci. U. S. A.* **2010**, *107*, 15335−15339.
(7) Tabares, L. C.; Un, S. *J. Biol. Chem.* **2013**, *288*, 5050−5055.
(8) Sharma, A.; Gaidamakova, E. K.; Matrosova, V. Y.; Bennett, B.; Daly, M. J.; Hoffman, B. M. *Proc. Natl. Acad. Sci. U. S. A.* **2013**, *110*, 5945−5950.
(9) Bruch, E. M.; de Groot, A.; Un, S.; Tabares, L. C. *Metallomics* **2015**, *7*, 908−916.
(10) Bruch, E. M.; Thomine, S.; Tabares, L. C.; Un, S. *Metallomics* **2015**, *7*, 136−144.
(11) Arieli, D.; Delabie, A.; Vaughan, D. E. W.; Strohmaier, K. G.; Goldfarb, D. *J. Phys. Chem. B* **2002**, *106*, 7509−7519.
(12) Schiemann, O.; Fritscher, J.; Kisseleva, N.; Sigurdsson, S. T.; Prisner, T. F. *ChemBioChem* **2003**, *4*, 1057−1065.
(13) Walsby, C. J.; Telser, J.; Rigsby, R. E.; Armstrong, R. N.; Hoffman, B. M. *J. Am. Chem. Soc.* **2005**, *127*, 8310−8319.
(14) Bennati, M.; Hertel, M. M.; Fritscher, J.; Prisner, T. F.; Weiden, N.; Hofweber, R.; Spörner, M.; Horn, G.; Kalbitzer, H. R. *Biochemistry* **2006**, *45*, 42−50.
(15) Schiemann, O.; Carmieli, R.; Goldfarb, D. *Appl. Magn. Reson.* **2007**, *31*, 543−552.
(16) LoBrutto, R.; Smithers, G. W.; Reed, G. H.; Orme-Johnson, W. H.; Tan, S. L.; Leigh, J. S. *Biochemistry* **1986**, *25*, 5654−5660.
(17) Bruch, E. M.; Warner, M. T.; Thomine, S.; Tabares, L. C.; Un, S. *J. Phys. Chem. B* **2015**, DOI: 10.1021/acs.jpcb.5b01624.
(18) Esteban-Gómez, D.; Cassino, C.; Botta, M.; Platas-Iglesias, C. *RSC Adv.* **2014**, *4*, 7094.
(19) Potapov, A.; Goldfarb, D. *Appl. Magn. Reson.* **2006**, *30*, 461−472.
(20) Davies, E. R. *Phys. Lett. A* **1974**, *47*, 1−2.
(21) Höfer, P. Entwicklung von Puls-ENDOR-Verfahren und ihre Anwendung auf Polyazetylen; Ph.D. Thesis, Universität Stuttgart, Stuttgart, Germany, 1988.
(22) Schosseler, P.; Wacker, T.; Schweiger, A. *Chem. Phys. Lett.* **1994**, *224*, 319−324.
(23) Frisch, M. J.; Trucks, G. W.; Schlegel, H. B.; Scuseria, G. E.; Robb, M. A.; Cheeseman, J. R.; Scalmani, G.; Barone, V.; Mennucci, B.; Petersson, G. A., et al. *Gaussian 09*, revision B.05; Gaussian, Inc.: Wallingford, CT, 2009.
(24) Neese, F. *Wiley Interdiscip. Rev. Comput. Mol. Sci.* **2012**, *2*, 73−78.
(25) Becke, A. D. *Phys. Rev. A: At., Mol., Opt. Phys.* **1988**, *38*, 3098−3100.
(26) Lee, C.; Yang, W.; Parr, R. G. *Phys. Rev. B: Condens. Matter Mater. Phys.* **1988**, *37*, 785−789.
(27) Becke, A. D. *J. Chem. Phys.* **1993**, *98*, 5648.
(28) Becke, A. D. *J. Chem. Phys.* **1993**, *98*, 1372.
(29) Ditchfield, R. *J. Chem. Phys.* **1971**, *54*, 724.
(30) Hehre, W. J.; Ditchfield, R.; Pople, J. A. *J. Chem. Phys.* **1972**, *56*, 2257.
(31) Rassolov, V. A.; Pople, J. A.; Ratner, M. A.; Windus, T. L. *J. Chem. Phys.* **1998**, *109*, 1223.
(32) Hariharan, P. C.; Pople, J. A. *Theor. Chim. Acta* **1973**, *28*, 213−222.
(33) Adamo, C.; Barone, V. *J. Chem. Phys.* **1999**, *110*, 6158.
(34) Tomasi, J.; Mennucci, B.; Cammi, R. *Chem. Rev.* **2005**, *105*, 2999−3094.
(35) Sinnecker, S.; Rajendran, A.; Klamt, A.; Diedenhofen, M.; Neese, F. *J. Phys. Chem. A* **2006**, *110*, 2235−2245.
(36) Schaftenaar, G.; Noordik, J. H. *J. Comput.-Aided Mol. Des.* **2000**, *14*, 123−134.
(37) Potapov, A.; Goldfarb, D. *Inorg. Chem.* **2008**, *47*, 10491−10498.
(38) Gillies, R. J.; Ugurbil, K.; den Hollander, J. A.; Shulman, R. G. *Proc. Natl. Acad. Sci. U. S. A.* **1981**, *78*, 2125−2129.

DOI: 10.1021/acs.inorgchem.5b01864
Inorg. Chem. 2015, 54, 10422−10428